ResearchGate

See discussions, stats, and author profiles for this publication at: https://www.researchgate.net/publication/231711567

Molecular Variables in the Self-Assembly of Supramolecular Nanostructures

ARTICLE *in* MACROMOLECULES · APRIL 2000

Impact Factor: 5.8 · DOI: 10.1021/ma9912756

CITATIONS
41

READS
12

4 AUTHORS, INCLUDING:

Paul Braun
University of Illinois, Urbana-Champaign
242 PUBLICATIONS **9,539** CITATIONS

SEE PROFILE

Available from: Paul Braun
Retrieved on: 25 January 2016

Molecular Variables in the Self-Assembly of Supramolecular Nanostructures

Martin U. Pralle, Craig M. Whitaker, Paul V. Braun, and Samuel I. Stupp*

Department of Materials Science and Engineering, Department of Chemistry, and Medical School, Northwestern University, Evanston, Illinois 60208

Received July 30, 1999; Revised Manuscript Received February 14, 2000

ABSTRACT: Supramolecular structures have the potential to provide macromolecular behavior using relatively low molar mass building blocks. We present here data on the self-assembly of triblock rodcoil molecules which contain a rigid biphenyl ester segment covalently linked to structurally diverse oligomeric segments. These molecules form supramolecular aggregates with molar masses in the range 10^5-10^6 Da, and our experiments probe how supramolecular structure can be manipulated by varying the volume fraction of the coillike flexible segments with respect to that of rod segments. The oligostyrene−oligoisoprene diblock coils were synthesized via anionic polymerization and varied in average length from (6_{sty}, 6_{iso}) to (30_{sty}, 30_{iso}). Small-angle X-ray scattering scans revealed layer spacings corresponding to monolayers that increase in size as the coil's molar mass increases. We observed that an increase in coil volume fraction reduces the thermal stability of the supramolecular structure, but a corresponding increase in rod segment length can counteract this effect. Finally the self-organized nanostructures seem to pack into a superlattice based on evidence obtained by X-ray scattering and transmission electron microscopy.

Introduction

We believe supramolecular assemblies of nanoscale dimension and molar mass in the range 10^5-10^6 Da could be useful in the design of novel functional materials. The challenge is to learn how to control the spontaneous formation of such large aggregates by encoding the size and shape information in precursor molecules. Our grasp of some of the variables that control nanostructure formation is essential to design libraries of functional materials. Since materials generally express their functionality in macroscopic forms, this vision requires also an understanding of the packing and networking of such nanostructures in three dimensions.

Supramolecular chemistry seeks to control the formation of intermolecular bonds and we are only beginning to discover the design rules behind noncovalent assembly. The formation of small aggregates of molecules was investigated by Whitesides and co-workers.[1−3] Also, Lehn[4] and Meijer[5] demonstrated the formation of 1D chains using small molecules. Supramolecular chemistry entered into nonlinear architectures in the high polymer regime with the discovery of 2D polymers[6,7] and mushroom shaped nanoaggregates in our laboratory[8] as well as other work including self-assembled blends,[9] dendritic polymers synthesized via self-assembly,[10−12] and finally polymerized self-organized vesicles.[13] These examples of nonlinear architectures are only a small fraction of the possibilities that supramolecular chemistry might offer in creating molecular object polymers. The ultimate goal herein should be to mimic the great functionality behind shape persistence in proteins.

Our laboratory has studied a variety of building blocks for materials in order to understand some of the central issues in the creation of supramolecular materials. We first reported on the combined use of self-organization and chemical reaction in chiral monomers to generate two-dimensional polymers.[6,7] We have also investigated the formation of nanostructures by self-assembly using rodcoil polymers,[14−16] so named because they have a rigid molecular segment covalently attached to a very flexible segment. Other work in the literature has focused on phase separation in high molecular weight rodcoil block copolymers.[17−19] Our work has targeted small molecules with rodcoil architecture as an approach to create nanoobjects with defined shapes. Furthermore, in contrast to conventional rodcoil polymers our rodcoil toolbox consists of molecules in which the rod segments have the molecular precision of organic compounds. Our recent report on these systems demonstrates they can form supramolecular materials with novel properties.

Crystallization and sterics in systems with rodcoil architecture are key factors in the formation of controlled supramolecular objects. We currently believe the energetic interplay between crystallization, coil entropy, and the repulsive energies associated with steric elements can lead to finite supramolecular objects with fairly defined size and shape. Biphenyl ester segments are the principal building blocks for the rigid rod segment, and these have a strong propensity to crystallize with $\pi-\pi$ stacked arrangements. In contrast, the oligostyrene and oligoisoprene coil segments are structurally diverse and hence unable to crystallize.[8] Finally the cross sectional area of the polystyrene chain is significantly larger than that of the biphenyl rod resulting in steric interactions. As these energetic terms balance, the size and shape of the supramolecular structure is defined. In this investigation, we have concentrated on the fundamental theme of understanding this energetic interplay. This was accomplished by varying the coil length and size as well as rod length and observing how such changes affect ordering behavior and structure.

* To whom correspondence should be addressed. This work was mostly carried out at the University of Illinois at Urbana−Champaign.

10.1021/ma9912756 CCC: $19.00 © 2000 American Chemical Society
Published on Web 04/29/2000

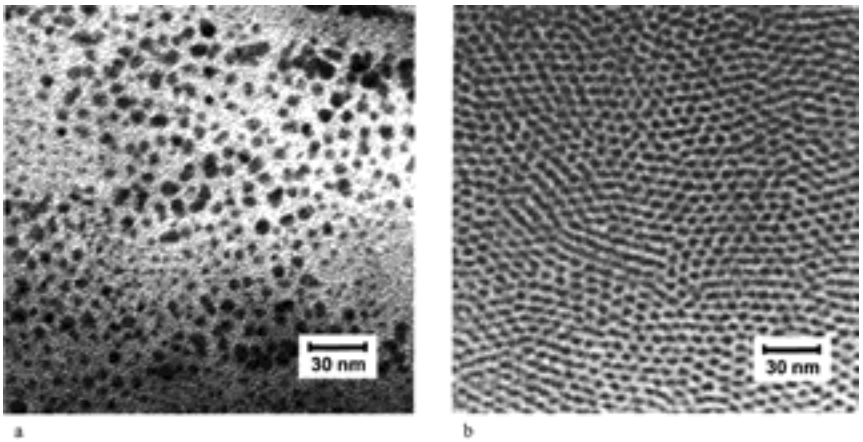

Figure 1. Transmission electron micrograph of rodcoil **1a** with an average of 6 units of isoprene and 6 units of styrene in the coil (a) and of **1b** with an average of 9 units of isoprene and 9 units of styrene (b). The shorter coil leads to more polydisperse and disordered nanostructures.

Table 1. Characterization of Rodcoil Materials

molecules	extended length (nm)	isotropization temp (°C)	SAXS *d* spacing (nm)
1a (6_{sty}, 6_{iso})	7.7	251	7.3
1b (9_{sty}, 9_{iso})	9.6	250	7.4
1c (13_{sty}, 14_{iso})	12.6	185	8.4
1d (12_{sty}, 20_{iso})	14.7	185	8.9
1e (20_{sty}, 12_{iso})	13.6	160	8.4
1f (30_{sty}, 30_{iso})	23.2	none	none

Results and Discussion

Rodcoils **1a**−**1f** were synthesized as described in the experimental procedure and then analyzed with polarized light microscopy, SAXS, and TEM to investigate

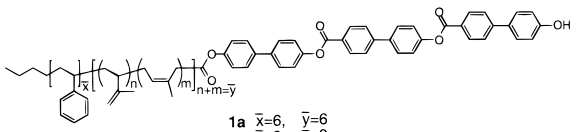

1a x̄=6, ȳ=6
1b x̄=9, ȳ=9
1c x̄=13, ȳ=14
1d x̄=12, ȳ=20
1e x̄=20, ȳ=12
1f x̄=30, ȳ=30

their solid state structure. These materials are birefringent solids under cross polarizers in the optical microscope. Upon heating, they undergo a transition to a liquid crystalline state followed by isotropization. In the liquid crystalline state, these materials are highly viscous suggesting a smetic phase, and this is also supported by their optical texture and small-angle X-ray diffraction. Interestingly, related work in our laboratory found evidence for the presence of aggregates in the liquid crystalline state.[20,21] As indicated in Table 1 the isotropization temperature of **1a** is 251 °C, similar to **1b**,[8] as measured by differential scanning calorimetry (DSC), a temperature that agrees with observations by optical microscopy. Interestingly, the isotropization peak is sharper and the corresponding heat of transition appears to be higher for **1b** vs **1a**. This is possibly a reflection of the higher order observed in **1b** (vida infra). In molecule **1c** the diblock coil length is changed to (13_{sty}, 14_{iso}), effectively increasing the coil to rod volume ratio, and the isotropization temperature decreases to 185 °C. The lower temperature for the phase transformation is indicative of a less stable ordered structure compared to **1a**. A further increase in coil length shows the same trend; **1e** (20_{sty}, 12_{iso}) clears at 160 °C and **1f** (30_{sty}, 30_{iso}) is a glass at room temperature and the material remains an isotropic medium until it decomposes above approximately 300 °C. Interestingly, however, reversing the relative lengths of the blocks in **1d**, with an average of 20 units of isoprene and 12 units of styrene results in a material with a isotropization temperature of 185 °C, nearly identical to that of **1c** even though its end-to-end calculated length is similar to **1e**.

X-ray studies of these materials were carried out in order to determine how the solid-state structure varied with the relative dimensions of the two blocks of the coil segment. SAXS scans of rodcoil films cast on glass from a 1 mg/mL chloroform solution and then annealed at 125 °C for 2 h showed interesting results. The (6_{sty}, 6_{iso}) derivative **1a** had a sharp SAXS peak at 73 Å, a similar periodicity to that of **1b** which revealed a (001) *d* spacing of 74 Å. The observation that increasing the coil length from (6_{sty}, 6_{iso}) to (9_{sty}, 9_{iso}) does not change the system's periodicity suggests that significant splaying of coils occurs over the rod clusters. It is important to note that from tilt angle calculations based on second harmonic generation experiments molecules **1b** are standing perpendicular to the layer.[22] The fact that layer periodicity does not drastically change from (9_{sty}, 9_{iso}) to (6_{sty}, 6_{iso}) coils also suggests that a certain extent of molecular stretching is forced on the system by rod crystallization. If the (6_{sty}, 6_{iso}) and (9_{sty}, 9_{iso}) systems have a similar volume of constrained segments, then the longer coils simply fold closer to the bottom of the nanostructures and do not change their height.

Characterization of rodcoil **1a** with TEM revealed the presence of nanocrystals (Figure 1). The samples were prepared without any special stains and therefore the contrast observed is due to diffraction and phase contrast in the samples themselves. Dark regions represent the crystallized rod clusters while the light regions surrounding each nanocrystal are regions containing the amorphous coil segments excluded from nanocrystals. Within some areas of the image the amorphous domains are too large to contain only a coil segment, and it is believed that these areas are comprised of rodcoils in a liquid crystalline glassy state.

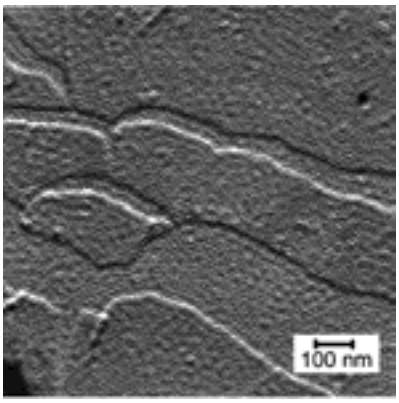

Figure 2. Transmission electron micrograph of a shadowed sample of **1a** (6_{sty}, 6_{iso}) showing the molecular steps in the film. The steps have thicknesses equal to the layer spacing observed in SAXS.

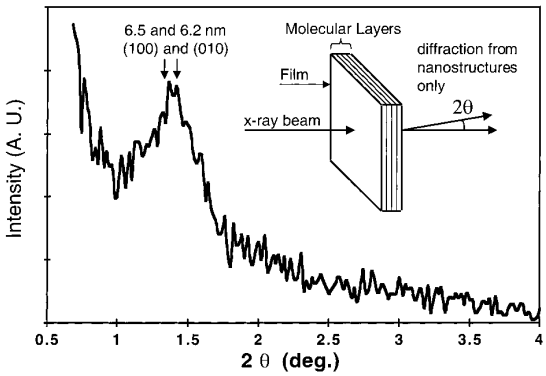

Figure 3. SAXS pattern of a rodcoil film taken perpendicular to the layers. The peak is indexed as both the (100) and (010) of the nanostructure superlattice.

Figure 1a shows a range of aggregate sizes for molecules **1a** from 4 to 7 nm. This was characteristically different from those observed in films of **1b** (Figure 1b) where the nanostructure dimensions are fairly monodisperse. The nanostructure polydispersity of **1a** effectively eliminated the possibility of a superlattice and hence the solid state is nonperiodic within one layer. It is possible that the strong variation in aggregate size is linked to polydispersity in chemical structure of coil segments. It is also possible that the lower coil to rod volume ratio leads to greater polydisperisty in aggregate size since the coil constrains the aggregate size. When the coil is smaller, there is less constraint and the polydispersity should increase. However, size diversity among nanostructures does not affect the system's strong propensity to self-organize into layers. In fact, the evidence for layering observed by SAXS was confirmed in electron micrographs of shadowed samples which reveal steps of the expected dimensions (72 Å) (see Figure 2). Finally, the nanostructures shown in Figure 1 were only observed in the thinnest regions of the film, presumably where the electron beam is passing through only one monolayer. This suggests that the layers observed in SAXS are comprised of nanostructures but there is little, if any, positional order of nanostructures from layer to layer. The lack of positional layer to layer registry in the structure would eliminate the possibility of observing nanostructures in thick portions of the film.

The superlattice of nanostructures observed via TEM by Stupp et al.[8] of **1b** reveals a high degree of regularity and long-range order. Such a structure should give rise to small angle scattering, yet this was not observed experimentally in powder SAXS scans. Since the superlattice repeat distances are nearly the same as the layer spacing, it is believed that the very intense (001) layer spacing reflection masks the (010) and (100) reflections from the superlattice. To support this hypothesis, SAXS scans were obtained with the X-ray beam directed perpendicular to molecular layers (see Figure 3). In this configuration, the diffraction from smectic layers is not at a Bragg condition and therefore the broad peak observed at 6.4 nm could be due to the nanostructure's lateral dimensions. The oblique superlattice observed by TEM has a unit cell with lattice parameters of 6.6 nm by 7.0 nm and an angle $\beta = 110°$.[8] Therefore, the broad scattering intensity centered at 6.4 nm can be indexed as two peaks corresponding to the (100) and (010) reflections with close agreement to the calculated values of 6.2 and 6.5 nm, respectively. The peak broadening could be due to a small coherence length as well as a lack of 3D ordering. As previously mentioned, there is limited correlation of the nanostructures in three dimensions as is evident by the drastic loss of contrast in TEM images of multilayer samples. We can therefore assume that nanostructures form 2D lattices layered on top of one another with no interlayer correlation. This structure would be very similar to those observed for DNA−lipid bilayer assemblies in which DNA chains form a 2D smectic phase but lack 3D correlation.[23−25] Reflections associated with the DNA smectic layers were observed experimentally[23,24] and predicted theoretically[25] to be broader and weaker in intensity due to the lack of correlation along the *z* direction. This behavior will manifest itself in our system by the broadening of both the (100) and the (010) reflections. Therefore, it is reasonable to suggest that the angular resolution of these reflections is lost and the peaks merge into one centered at 1.4 deg in 2θ.

To investigate the thermodynamic stability of the layered structures formed by the triblock self-assembling molecules of interest here, a variable temperature experiment was carried out. By rapid precipitation of **1b** out of chloroform solution through the addition of methanol, an amorphous glassy solid forms. Interestingly, however, upon annealing the system rapidly self-organizes into a layered structure. This is clearly revealed by the variable temperature SAXS scans shown in Figure 4. Note the lack of order at 23 and 75 °C and the subsequent appearance of a peak corresponding to a *d* spacing of 74 Å at higher temperatures. This peak continues to rise in intensity as the temperature is increased, and at 250 °C it disappears, in agreement with observations by optical microscopy which indicate that isotropization occurs between 225 and 250 °C. Most importantly, if the sample is slowly cooled from 200 °C the order remains, implying that the stable organization at room temperature is layered and not glassy. Furthermore, molecule-solvent interactions should play an important role in the kinetics of self-assembly in these systems.

SAXS of **1c** reveals a sharp peak at 84 Å as well as a broad and very weak peak corresponding to a *d* spacing of 50 Å. The broad peak at 50 Å is possibly associated with the distance between nanoaggregates within the plane of the film. The (001) *d* spacing increases as the

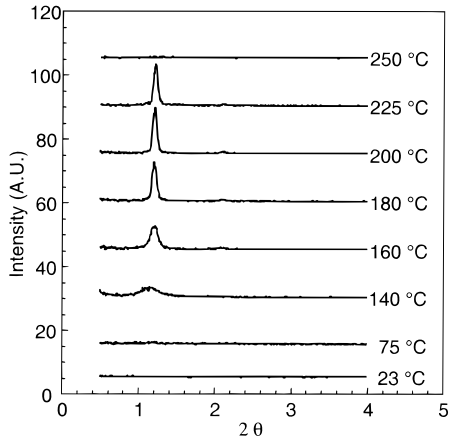

Figure 4. Variable temperature SAXS of a rodcoil kinetically trapped in the glassy state. As the temperature is increased the material softens and the layered morphology rapidly forms.

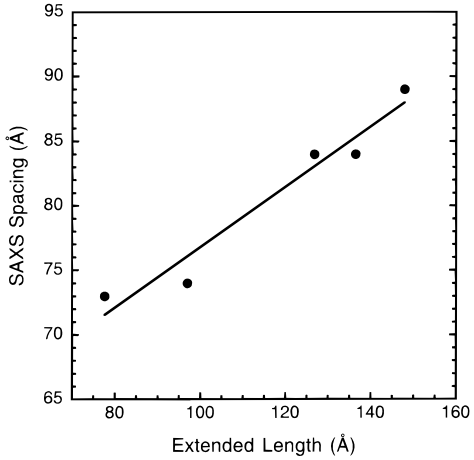

Figure 5. Plot showing the linear relationship between molecular spacing in the solid state and the extended length of the molecule. The extended length is directly proportional to the degree of polymerization.

coil structure is changed from (9_{sty}, 9_{iso}) to (13_{sty}, 14_{iso}) in **1b** and **1c** respectively, an expected result considering the increase in molecular length. A further increase in coil length in **1d** and **1e** results in greater layer periodicities. Figure 5 shows a plot of the layer periodicity in **1a**−**1f**, which reflects the height of nanostructures, as a function of the extended length of the corresponding average-sized molecules. The first important feature of the plot in Figure 5 is the fact that *d* spacings are always significantly smaller than extended molecular lengths. This observation offers partial evidence for the mushroom-like nature of the nanostructures lacking $D_{\infty h}$ symmetry. In other words, the plot would not support the formation of dumbell-like symmetric nanostructures formed either through interdigitation of the rod segments or through strong stem-to-stem interactions between two mushroomlike nanostructures. Such packing arrangements would generate larger *d* spacings in SAXS scans. Also, these packing arrangements do not successfully fill free volume as was discussed elsewhere.[8] Second, the deviation from a slope of 1 suggests that partial folding of coils occurs over the rod clusters thus defining the mushroom architecture. Therefore, infinite layers of nearly extended molecules, as commonly occurs in smectic phases, do not seem to form here. The implication is that finite supramolecular clusters are the basic constituents of these solids. Interestingly, the linearity of the data strongly suggests non-Gaussian behavior within the coils providing insight into the constrained environment these chains experience, for example, stretching of flexible units attached to rod segments.

We investigated the self-assembling behavior of a rodcoil system containing a shorter rod segment than all other materials studied here. The first rodcoil synthesized was the (9_{sty}, 9_{iso}) system with only two biphenyl units in the rod segment (**2**). SAXS of **2** showed

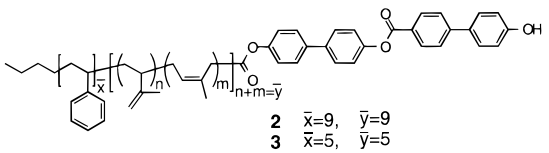

2 x̄=9, ȳ=9
3 x̄=5, ȳ=5

a weak, broad signal at 70 Å but these molecules do not appear to have the same strong ordering ability as the 3 biphenyl unit homologues (**1b**). Therefore, molecules were synthesized which contained the same number of biphenyl units as **2** and coil lengths of only (5_{sty}, 5_{iso}) (**3**). After annealing, rodcoil **3** showed a sharp SAXS (001) peak at 60 Å and an (002) peak at 30 Å. When the coil length remains the same but only 1-biphenyl unit is attached to the coil (**4**), the material does not

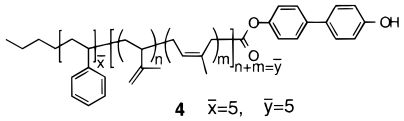

4 x̄=5, ȳ=5

form an ordered solid as revealed by the absence of birefringence when examined under the optical microscope.

Transmission electron microscopy studies of **3** gave interesting results. The micrograph (Figure 6) shows 20−25 nm aggregates dispersed throughout the film. The electron diffraction inset shows that these aggregates are crystalline with a unit cell identical to **1b** (orthorhombic with lattice parameters $a = 8.2$ Å and $b = 5.6$ Å). The 20−25 nm crystalline aggregates are much larger than those observed in **1b** (5 nm aggregates). This suggests that repulsive forces among the short (5_{sty}, 5_{iso}) coil segments are dramatically reduced allowing further growth of the crystalline aggregates of rod segments. However, not all of the material forms these crystallites as can be observed in the micrograph (the micrograph was taken at focus with an objective aperture). The objective aperture generates contrast by eliminating diffracted beams while maintaining transmitted beams. In this configuration, any species that strongly diffracts electrons appears dark (the aggregates observed) and the lighter regions that transmit a majority of the electrons are amorphous. This amorphous component is also observable in the electron diffraction pattern where an amorphous halo is clearly visible. The aggregate−aggregate spacing is ∼50 nm, a distance far larger than that which can be attributed to the stretching and splaying of the coils. Therefore, there must be noncrystalline material within this region. Perhaps the short segments of the Poisson distribution are aggregat-

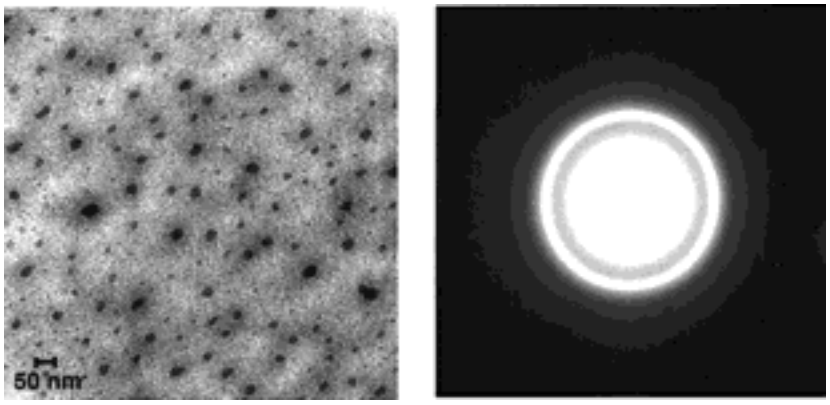

Figure 6. TEM (a) and electron diffraction pattern (b) of a rodcoil with a short 2 biphenyl rod and a short 5 unit oligostyrene, 5 unit oligoisoprene coil. The image is unstained, and therefore the contrast is derived from diffraction and phase contrast. The electron diffraction pattern shows Debye rings corresponding to the (110), (200), and the (210) reflections.

ing and crystallizing while the longer segments remain a liquid crystalline glass.

We mentioned previously that **1f** (30_{sty}, 30_{iso} coil, 3-biphenyl rod) did not spontaneously self-assemble and does not give rise to small angle scattering. The lack of ordering behavior in these molecules was predicted to be due to the dominating entropic and van der Waals energetic contribution of the coils over the relatively smaller enthalpic contribution to the free energy by crystallized rods. Rodcoil **5** with 4-biphenyl units and

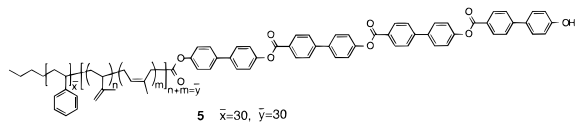

5 $\bar{x}$=30, $\bar{y}$=30

(30_{sty}, 30_{iso}) coil was therefore synthesized to test this hypothesis. Rodcoil **5** has a higher clearing temperature at 300 °C than the shorter coil derivatives. SAXS scans showed a sharp peak at 100 Å and a broader peak at 60 Å which we attribute to nanostructure packing within the layer. In so doing we have effectively counteracted the disruptive steric interactions of bulky long coil segments. This critical transition seems to occur consistently in the range of 0.85−0.9 coil volume fraction. However, we expect that this is a nonlinear relationship since longer rods may have significantly higher enthalpies of crystallization. This observation is important because it demonstrates that the coil-to-rod ratio is a key variable in the formation of self-organized rodcoil nanostructures.

Conclusions

Triblock rodcoil molecules offer rich systems to study self-assembly over many length scales. The height of the anisometric nanostructures they form scales linearly with molar mass but it is always significantly less than the extended length of triblock molecules. This is consistent with the formation of "mushroom"-shaped nanostructures in which coils can randomly splay over the crystalline rod packet. We have demonstrated that rod to coil volume ratios determine if self-assembly occurs, and as expected large coil volumes reduce the thermal stability of the ordered state. We have also observed the complete disruption of layered structures as the coil volume fraction is increased beyond a critical value.

Experimental Section

The ^{1}H and ^{13}C NMR spectra were obtained using Varian U400 and U500 spectrometers in the indicated solvents; chemical shifts are expressed in parts per million (δ) using residual solvent protons as an internal standard. Splitting patterns are designated as follows: s = singlet, d = doublet, t = triplet, q = quartet, qu = quintet, m = multiplet, and b = broad. Analytical thin-layer chromatography (TLC) was performed on KIESELGEL F-254 precoated TLC plates. Silica for column chromatography was Silica Gel 60 (230−400 mesh) from EM Science. Gel permeation chromatography (GPC) analyses were performed in THF using a Waters 600E instrument equipped with UV and refractive index detectors. Differential scanning calorimetry (DSC) was carried out in a TA instruments model 2920 calorimeter and in all scans heating and cooling rates were 10 °C/min. Polarized optical microscopy utilized a Leitz Laborlux 12POL optical microscope equipped with a Linkham THM 600 hot stage. Samples were kept under nitrogen at elevated tempertures. Small-angle X-ray scattering (SAXS) was carried out on a Siemens Anton Paar high-resolution small angle camera equipped with a Hi-Star area detector and Bruker (Siemens) SAXS software mounted on an M18X-HF22 SRA rotating anode generator. Powder diffraction rings were integrated over 360° to yield the patterns and were calibrated using a silver beheanate standard. Transmission electron microscopy (TEM) studies were performed on a Phillips CM 200 TEM operating at 120 keV accelerating voltage using bright field imaging. Samples were prepared by casting from chloroform solution onto a water surface and then transferring the resulting films to copper TEM grids and analyzed without annealing. The samples are beam sensitive, and contrast is lost during longer electron beam exposures.

Unless otherwise noted, all starting materials were obtained from Aldrich and used without further purification. Dry styrene, isoprene, dichloromethane, and *N*,*N*-dimethylformamide (DMF) were obtained by vacuum transfer from calcium hydride. Dry tetrahydrofuran (THF) and benzene were obtained by vacuum transfer from sodium and benzophenone. Diisopropylcarbodiimide (DIPC) was distilled before use. 4-(*N*,*N*-Dimethylamino)pyridinium-4-toluenesulfonic acid (DPTS) was prepared using a published procedure.[26]

4′-Hydroxy-4-(dimethylthexylsilyloxybiphenyl) Carboxylate. Morpholine (2.2 mL, 23.0 mmol, *d* 0.999), 4′-hydroxy-4-biphenyl carboxylic acid (5.0 g, 23.3 mmol), and dimethylformamide (20 mL) were placed in a flask and stirred. (Dimethylthexyl)silyl chloride (4.5 mL, 23.0 mmol, *d* 0.909) was added and the solution was stirred at room temperature for 30 min. The resulting mixture was diluted with dichloromethane (100 mL), washed with saturated aqueous sodium bicarbonate (200 mL), and water (200 mL), and then dried over $MgSO_4$. The solvent was removed by rotatory evaporation and the product was purified by column chromatography (CH_2Cl_2)

to give a tacky, white solid. Yield: 7.3 g (80%). ^{1}H NMR ($CDCl_3$): δ 8.09 (d, 2H), 7.62 (d, 2H), 7.52 (d, 2H), 7.00 (d, 2H), 6.90 (br, 1H), 1.81 (m, 1H), 0.97 (m, 12H), 0.48 (s, 6H).

(6,6)-Carboxylated Oligo(styrene-*b*-isoprene). Benzene (50 mL), THF (5 mL), and styrene (5 mL, 43.7 mmol, *d* 0.909) were placed in a flask and the solution was degassed by a freeze−pump−thaw cycle using liquid nitrogen. *n*-BuLi (1.6 M in hexanes, 3.9 mL, 6.2 mmol) was added with rapid stirring.[27] The resulting deep red solution was stirred at room temperature for 2 h, and then isoprene (5.0 mL, 46.0 mmol, *d* 0.627) was added to the solution. The yellow solution was stirred for an additional 2 h. The reaction was quenched by bubbling carbon dioxide through the solution for 5 min. Acidic methanol (5 mL) was added to the now clear solution, and then the solvent was removed by rotatory evaporation to give a tacky solid. The product was isolated via column chromatography using first CH_2Cl_2 (1500 mL) as the eluent to remove any impurities, and then acetone (1500 mL) to give the desired product. Yield: 1.2 g (17%). ^{1}H NMR ($CDCl_3$): δ 6.35−7.2 (m, 45H, styrene aromatic), 4.4−5.2 (m, 12H, isoprene vinylic), 0.8−3.2 (m, 110H, aliphatic). GPC (THF): PDI 1.05; M_n 1700. Different lengths of the oligostyrene-*b*-isoprene coil segements, (5, 5), (13, 15), (12, 20), (20, 12), and (30, 30), were made by altering the ratio of the *n*-butyl−Li to the styrene and isoprene monomers.

4′-Bromo-4-(dimethylthexylsilyloxy)biphenyl. A dry flask was charged with 4′-bromo-4-hydroxybiphenyl (10 g, 40.2 mmol), imidazole (2.9 g, 42.2 mmol), and dichloromethane (100 mL). After stirring for 10 min, dimethylthexylsilyl chloride (8.3 mL, 42.2 mmol, *d* 0.909) was added dropwise. The solution was stirred overnight at room temperature, and then diluted with dichloromethane (100 mL) and washed with saturated aqueous sodium bicarbonate (200 mL), and water (200 mL). The organic layers were then dried over $MgSO_4$ and filtered and the solvent removed by rotatory evaporation. The product was purified using column chromatography (1:1 petroleum ether, CH_2Cl_2). Yield: 15.0 g (95%). ^{1}H NMR ($CDCl_3$): δ 7.56 (d, 2H), 7.44 (dd, 2H), 6.95 (d, 2H), 1.81 (m, 1H), 1.03 (s, 12 H), 0.32 (s, 6H).

4′-(Dimethylthexylsilyloxy)-4-(4′-hydroxy-4-biphenyl) Carboxylate. A flask was charged with 4′-hydroxy-4-(dimethylthexylsilyloxy carboxylate)biphenyl (5.0 g, 14.0 mmol), 4,4′-biphenol (10.5 g, 56.1 mmol), DPTS (3.8 g, 14.0 mmol), and DMF (100 mL). Diisopropylcarbodiimide (DIPC, 2.1 mL, 13.6 mmol, *d* 0.806) was added and the mixture was stirred at room temperature for 24 h. The mixture was then diluted with water (200 mL) and extracted with dichloromethane (200 mL). The organic layers were combined and dried over $MgSO_4$, and the solvent was removed by rotatory evaporation. The product was purified by column chromatorgraphy (1:10 MeOH, CH_2Cl_2) as a white solid. Yield: 5.0 g (69%). ^{1}H NMR ($CDCl_3$): δ 8.28 (d, 2H), 7.70 (d, 2H), 7.58 (d, 4H), 7.42 (d, 2H), 7.27 (d, 2H), 6.98 (d, 2H), 6.92 (d, 2H), 5.44 (br, 1H), 1.01 (s, 12H), 0.22 (s, 6H).

4′-(Dimethylthexylsilyloxy)-4-biphenylcarboxylic Acid. Magnesium turnings (1.9 g, 76.8 mmol) and diethyl ether (100 mL) were placed in a round-bottom flask. 4′-Bromo-4-(dimethylthexylsilyloxy)biphenyl (10.0 g, 25.6 mmol), ethyl bromide (3.82 mL, 51.2 mmol, *d* 1.460) and diethyl ether (100 mL) were added to the stirred mixture as the solvent was refluxed. Once the addition was complete, the mixture was refluxed for an additional 2 h. The reaction was quenched with dry carbon dioxide for 5 min, and then the solution was decanted away from the unreacted magnesium turnings. The ether solution was washed with 1 N HCl (200 mL) and water (500 mL) and then dried over $MgSO_4$. The solvent was removed by rotatory evaporation, and then the solid was taken up in an excess of petroleum ether (300 mL). The mixture was filtered, and the product was collected via vacuum filtration as a white solid. Yield: 7.3 g (80%). ^{1}H NMR ($CDCl_3$): δ 8.19 (d, 2H), 7.63 (d, 2H), 7.54 (d, 2H), 6.92 (d, 2H), 1.79 (m, 1H), 0.98 (s, 12H), 0.23 (s, 6H).

4′-[[4′-(Dimethylthexylsilyloxy)-4-biphenyl]carbonyloxy]-biphenyl Poly(styrene-*b*-isoprene) 4-Carboxylate. Carboxylated poly(styrene-*b*-isoprene) (1.0 g, 0.7 mmol), 4′-(dimethylthexylsilyloxy)-(4′-hydroxy-4-biphenyl) 4-carboxylate (0.36 g, 0.7 mmol), DPTS (0.23 g, 0.8 mmol) and dichloromethane (10 mL) were placed in a flask. Diisopropylcarbodiimide (0.5 mL, 0.8 mmol, *d* 0.806) was added, and the solution was stirred overnight at room temperature. The resulting precipitate was removed via filtration, and the solvent was removed by rotatory evaporation. The product was isolated by column chromatorgraphy (CH_2Cl_2) as a white solid. Yield: 1.1 g (80%). ^{1}H NMR ($CDCl_3$): δ 8.32 (d, 2H), 7.68 (d, 2H), 7.60 (m, 4H), 7.38 (d, 2H), 7.30 (d, 2H), 6.35−7.25 (m, 50 H), 4.41−5.26 (m, 12H), 1.01−2.41 (m, 116H), 0.92 (s, 12H), 0.30 (s, 6H). GPC (THF): PDI 1.07; M_n 1920.

4′-[(4′-Hydroxy-4-biphenyl)carbonyloxy]biphenyl Poly(styrene-*b*-isoprene) 4-Carboxylate (2 and 3). Tetrahydrofuran (20 mL) and 4′-[[4′-(dimethylthexylsilyloxy)-4-biphenyl]-carbonyloxy]biphenyl poly(styrene-*b*-isoprene) 4-carboxylate (1.1 g, 0.5 mmol) were placed in a round-bottom flask and cooled to −78 °C in a dry ice/acetone slush bath. *tert*-Butylammonium fluoride (TBAF, 1.0 N solution in THF, 3.0 mL) was added dropwise, and the solution was stirred at −78 °C for 3 h; then another portion of TBAF (1.0 mL) was added, and stirring was continued for 1 h. The reaction mixture was quenched with a solution of acetic acid (0.2 g) in THF (15 mL) at −78 °C. The contents were poured into dichloromethane (100 mL) and washed with brine (150 mL) and water (150 mL). The organic layer was dried over $MgSO_4$, and the solvent was removed by rotatory evaporation. The product was purified by column chromatography (1:10 MeOH, CH_2Cl_2) to give a white solid. Yield: 1.07 g (98%). ^{1}H NMR ($CDCl_3$): δ 8.32 (d, 2H), 7.69 (d, 2H), 7.62 (m, 4H), 7.39 (d, 2H), 7.33 (d, 2H), 6.35−7.25 (m, 50 H), 4.41−5.26 (m, 12H), 1.01−2.41 (m, 116H). GPC (THF): PDI 1.05; M_n 1860 (9, 9). GPC (THF): PDI 1.10; M_n 1540 (5, 5).

4′-[4′[[4′-(Dimethylthexylsilyloxy)-4-biphenyl]carbonyloxy]-4-biphenylcarbonyloxy]biphenyl Poly(styrene-*b*-isoprene) 4-Carboxylate. A solution of 4′-dimethylthexylsilyloxy-4-biphenylcarboxylic acid (1.0 g, 0.5 mmol), 4′-[(4′-hydroxy-4-biphenyl)carbonyloxy]biphenyl [poly(styrene-*b*-isoprene)-4-carboxylate (0.2 g, 0.6 mmol), DPTS (0.2 g, 0.8 mmol), and dichloromethane (20 mL) was stirred at room temperature for 5 min. Diisopropylcarbodiimide (0.5 mL, 1.6 mmol, *d* 0.806) was added dropwise, and the solution was stirred overnight at room temperature. The solution was diluted with dichloromethane (30 mL) and then washed with water (50 mL). The organic layer was dried over $MgSO_4$, and then the solvent was removed by rotatory evaporation. The product was isolated by column chromatography (CH_2Cl_2) as a white solid. Yield: 0.95 g (78%). ^{1}H NMR ($CDCl_3$): δ 8.32 (d, 2H), 8.26 (d, 2H), 7.75 (d, 2H), 7.68 (m, 2H), 7.60 (d, 4H), 7.52 (d, 2H), 7.38 (d, 2H), 7.30 (d, 2H), 6.35−7.25 (m, 50 H), 4.41−5.26 (m, 12H), 1.01−2.41 (m, 116H), 0.92 (s, 12H), 0.30 (s, 6H). GPC (THF): PDI 1.07; M_n 2080.

4′-[4′-[4′-(Hydroxy-4-biphenyl)carboyloxy]-4-biphenyl carbonyloxy]biphenyl Poly(styrene-*b*-isoprene) 4-Carboxylate (1b). A flask was charged with 4′-[4′[[4′-(Dimethylthexylsilyloxy)-4-biphenyl]carbonyloxy]-4-biphenyl carbonyloxy] biphenyl poly(styrene-*b*-isoprene) 4-carboxylate (0.9 g, 0.4 mmol) and THF (20 mL). The solution was cooled to −78 °C in a dry ice/acetone slush bath, then TBAF (1.0 N solution in THF, 3.0 mL) was added slowly and the reaction mixture was stirred for 3 h. A second portion of TBAF (1.0 mL) was then added, and the solution was stirred for 1 h at −78 °C. The reaction mixture was quenched with a solution of acetic acid (0.2 g) in THF (15 mL) at −78 °C. The contents were poured into dichloromethane (100 mL) and washed with water (100 mL). The organic layer was dried over $MgSO_4$, then the solvent was removed by rotatory evaporation. The product was isolated by column chromatography (1:10, MeOH/CH_2Cl_2) as a white solid. Yield: 0.81 g (97%). ^{1}H NMR ($CDCl_3$): δ 8.33 (d, 2H), 8.29 (d, 2H), 7.77 (d, 2H), 7.69 (m, 2H), 7.62 (d, 4H), 7.55 (d, 2H), 7.37 (d, 2H), 7.31 (d, 2H), 6.35−7.25 (m, 48 H), 4.41−5.26 (m, 12H), 1.01−2.41 (m, 113H).

4-Biphenylcarbonyloxy Poly(styrene-*b*-isoprene) (4). Carboxylated poly(styrene-*b*-isoprene) (1.0 g, 0.7 mmol),

biphenol (0.13 g, 0.7 mmol), DPTS (0.23 g, 0.8 mmol), and dichloromethane (10 mL) were placed in a flask. Diisopropylcarbodiimide (0.5 mL, 0.8 mmol, *d* 0.806) was added, and the solution was stirred overnight at room temperature. The resulting precipitate was removed via filtration, and the solvent was removed by rotatory evaporation. The product was isolated by column chromatorgraphy (CH_2Cl_2) as a white solid. Yield: 0.9 g (65%). ^{1}H NMR ($CDCl_3$): δ 7.68 (d, 2H), 6.35−7.25 (m, 32 H), 4.41−5.26 (m, 7H), 1.01−2.41 (m, 70H).

4′-[4′-[4′-(Dimethylthexylsilyloxy)-4-biphenyl]carbonyloxy]-4-biphenyl carbonyloxy]biphenyl Poly(styrene-*b*-isoprene) 4-Carboxylate. A solution of 4′-dimethylthexylsilyloxy-4-biphenylcarboxylic acid (1.0 g, 0.5 mmol), 4′-[(4′-hydroxy-4-biphenyl)carbonyloxy]biphenyl poly(styrene-*b*-isoprene) 4-carboxylate (0.2 g, 0.6 mmol), DPTS (0.2 g, 0.8 mmol), and dichloromethane (20 mL) was stirred at room temperature for 5 min. Diisopropylcarbodiimide (0.5 mL, 1.6 mmol, *d* 0.806) was added dropwise, and the solution was stirred overnight at room temperature. The solution was diluted with dichloromethane (30 mL), then washed with water (50 mL). The organic layer was dried over $MgSO_4$, then the solvent was removed by rotatory evaporation. The product was isolated by column chromatography (CH_2Cl_2) as a white solid. Yield: 0.95 g (78%). ^{1}H NMR ($CDCl_3$): δ 8.32 (d, 4H), 8.26 (d, 4H), 7.75 (d, 4H), 7.68 (m, 2H), 7.60 (d, 4H), 7.52 (d, 2H), 7.38 (d, 2H), 7.30 (d, 2H), 6.35−7.25 (m, 50 H), 4.41−5.26 (m, 12H), 1.01−2.41 (m, 116H), 0.92 (s, 12H), 0.30 (s, 6H). GPC (THF): PDI 1.07; M_n 5100.

4′-[4′-[4′-[4′-Hydroxy-4-biphenyl]carbonyloxy]-4-biphenylcarbonyloxy]biphenyl Poly(styrene-*b*-isoprene) 4-Carboxylate (5). A flask was charged with 4′-[4′-[4′[4′-(Dimethylthexylsilyloxy)-4-biphenyl]carbonyloxy]-4-biphenylcarbonyloxy]biphenyl poly(styrene-*b*-isoprene) 4-carboxylate (0.9 g, 0.4 mmol) and THF (20 mL). The solution was cooled to −78 °C in a dry ice/acetone slush bath, and then TBAF (1.0 N solution in THF, 3.0 mL) was added slowly and the reaction mixture was stirred for 3 h. A second portion of TBAF (1.0 mL) was then added, and the solution was stirred for 1 h at −78 °C. The reaction mixture was quenched with a solution of acetic acid (0.2 g) in THF (15 mL) at −78 °C. The contents were poured into dichloromethane (100 mL) and washed with water (100 mL). The organic layer was dried over $MgSO_4$, and then the solvent was removed by rotatory evaporation. The product was isolated by column chromatography (1:10, MeOH/CH_2Cl_2) as a white solid. Yield: 0.81 g (97%). ^{1}H NMR ($CDCl_3$): δ 8.33 (d, 4H), 8.29 (d, 4H), 7.77 (d, 4H), 7.69 (m, 2H), 7.62 (d, 4H), 7.55 (d, 2H), 7.37 (d, 2H), 7.31 (d, 2H), 6.35−7.25 (m, 48 H), 4.41−5.26 (m, 12H), 1.01−2.41 (m, 113H).

Acknowledgment. This work was supported by grants from the National Science Foundation (DMR 9996253), the Office of Naval Research (N00014-98-1-0239), and the Department of Energy (DEFG02-96-ER45439). We acknowledge use of the Visualization Laboratory of the Beckman Institute for Advanced Science and Technology at the University of Illinois. The authors are grateful to Li Sheng Li for help with some of the TEM experiments.

References and Notes

(1) Whitesides, G. M.; Mathias, J. P.; Seto, C. T. *Science* **1991**, *254*, 1312−1319.
(2) Mathias, J. P.; Simanek, E. E.; Whitesides, G. M. *J. Am. Chem. Soc.* **1994**, *116*, 4326−4340.
(3) Seto, C. T.; Mathias, J. P.; Whitesides, G. M. *J. Am. Chem. Soc.* **1993**, *115*, 1321−1329.
(4) Lehn, J. M. *Supramolecular Chemistry*; VCH Press: New York, 1995.
(5) Hirschberg, J. H. K. K.; Beijer, F. H.; van Aert, H. A.; Magusim, P. C. M. M.; Sijbesma, R. P.; Meijer, E. W. *Macromolecules* **1999**, *32*, 2696−2705.
(6) Stupp, S. I.; Son, S.; Lin, H. C.; Li, L. S. *Science* **1993**, *259*, 59−63.
(7) Stupp, S. I.; Son, S.; Li, L. S.; Lin, H. C.; Keser, M. *J. Am. Chem. Soc.* **1995**, *117*, 5212−5227.
(8) Stupp, S. I.; LeBonheur, V.; Walker, K.; Li, L. S.; Huggins, K.; Keser, M.; Amstutz, A. *Science* **1997**, *276*, 384−389.
(9) Kihara, H.; Kato, T.; Uryu, T.; Frechet, J. M. J. *Chem. Mater.* **1996**, *8*, 961−968.
(10) Percec, V.; Ahn, C. H.; Ungar, G.; Yeardley, D. J. P.; Moller, M.; Sheiko, S. S. *Nature* **1998**, *391*, 161−164.
(11) Hudson, S. D.; Jung, H. T.; Percec, V.; Cho, W. D.; Johansson, G.; Ungar, G.; Balagurusamy, V. S. K. *Science* **1997**, *278*, 449−452.
(12) Zimmerman, S. C.; Zeng, F.; Reichert, D. E. C.; Kolotuchin, S. V. *Science* **1996**, *271*, 1095−1098.
(13) Thurmond, K. B.; Kowalewski, T.; Wooley, K. L. *J. Am. Chem. Soc.* **1997**, *119*, 6656−6665.
(14) Radzilowski, L. H.; Wu, J. L.; Stupp, S. I. *Macromolecules* **1993**, *26*, 879−882.
(15) Radzilowski, L. H.; Stupp, S. I. *Macromolecules* **1994**, *27*, 7747−7753.
(16) Radzilowski, L. H.; Carragher, B. O.; Stupp, S. I. *Macromolecules* **1997**, *30*, 2210−2119.
(17) Ober, C. K.; Wegner, G. *Adv. Mater.* **1997**, *9*, 17−31.
(18) Jenekhe, S. A.; Chen, X. L. *Science* **1999**, *283*, 372−375.
(19) Li, W.; Wan, H.; Yu, L. P.; Morkved, T. L.; Jaeger, H. M. *Macromolecules* **1999**, *32*, 3034−3044.
(20) Zubarev, E. R.; Pralle, M. U.; Li, L.; Stupp, S. I. *Science* **1999**, *283*, 523−526.
(21) Tew, G. N.; Pralle, M. U.; Stupp, S. I. *J. Am. Chem. Soc.* **1999**, *121*, 9852−9866.
(22) Li, L.; Stupp, S. I. Unpublished results.
(23) Radler, J.; Koltover, I.; Salditt, T.; Safinya, C. R. *Science* **1997**, *275*, 810.
(24) Salditt, T.; Koltover, I.; Radler, J.; Safinya, C. R. *Phys. Rev. E* **1998**, *58*, 889.
(25) O'Hern, C. S.; Lubensky, T. C. *Phys. Rev. Lett.* **1998**, *23*, 65−70.
(26) Moore, J. S.; Stupp, S. I. *Macromolecules* **1990**, *23*, 65−70.
(27) Swzarc, M. *Carbanions, Living Polymers, and Electron-Transfer Processes*; Wiley: New York, 1968.

MA9912756